Harvesting Wind Energy Using a Galloping Piezoelectric Beam

Jayant Sirohi
Assistant Professor
e-mail: jayant.sirohi@mail.utexas.edu

Rohan Mahadik
Graduate Research Assistant

Department of Aerospace Engineering and Engineering Mechanics,
The University of Texas at Austin,
1 University Station, C0600,
Austin, TX 78712-0235

Galloping of structures such as transmission lines and bridges is a classical aeroelastic instability that has been considered as harmful and destructive. However, there exists potential to harness useful energy from this phenomenon. This paper focuses on harvesting wind energy that is being transferred to a galloping beam. The beam has a rigid tip body with a D-shaped cross section. Piezoelectric sheets are bonded on the top and bottom surface of the beam. During galloping, vibrational motion is input to the system due to aerodynamic forces on the D-section, which is converted into electrical energy by the piezoelectric (PZT) sheets. The relative importance of various parameters of the system such as wind speed, material properties of the beam, electrical load and beam's natural frequency are discussed. Experimental and analytical investigations of dynamic response and power output are performed on a representative device. A maximum output power of 1.14 mW was measured at a wind velocity of 10.5 mph on a prototype device of length 235 mm and width 25 mm. A potential application for this device is to power wireless sensor networks on outdoor structures such as bridges and buildings. [DOI: 10.1115/1.4004674]

1 Introduction

Galloping of a structure is characterized as a phenomenon involving low frequency, large amplitude oscillations normal to the direction of incident wind. Typically, it occurs in lightly damped structures with asymmetric cross sections. Galloping is caused by a coupling between aerodynamic forces acting on the structure and the structural deflections. Significant research has been done in the past to study various parameters influencing galloping behavior of structures with different cross-sections, such as, rectangular, prismatic, D-section, and triangular. A classic example is the galloping of ice-covered transmission lines.

Den Hartog [1] explained the phenomenon of galloping for the first time in 1934 and introduced a criterion for galloping stability of a structure. Alonso et al. [2] conducted experiments on a prismatic bar with triangular cross-section, mounted on an elastic support. He determined the aerodynamic coefficients (sectional lift and drag) of the cross-section and demonstrated the dependence of quasi-steady angle of attack on the occurrence of galloping. Kazakevich and Vasilenko [3] determined the dependence of galloping amplitude on incident wind velocity by means of a closed form analytical solution for a bar with rectangular cross-section. Experimental results obtained by Laneville et al. [4] on a D-section exposed to turbulent flow show that it is highly prone to galloping at higher angles of attack. These past studies have established the influence of various parameters such as wind velocity, cross-sectional geometry of the structure and angle of attack, on galloping.

The structural vibrations induced by galloping can be beneficial if converted into a useful form of energy. There have been limited studies in past on harvesting energy from aerodynamic instabilities. Barrero-Gil et al. [5] theoretically investigated the feasibility of energy harvesting from structures undergoing galloping. They represented the sectional aerodynamic characteristics using a cubic polynomial and obtained an expression for the harnessable energy. Specific methods for energy extraction were not discussed. Robbins et al. [6] investigated the use of flexible, flaglike, piezoelectric sheets to generate power while flapping in an incident wind. Wang and Ko [7] carried out studies to harvest energy from a piezoelectric sheet excited by flow-induced pressure fluctuations. Their design generates an output power of 0.2 μW in response to a pressure fluctuation occurring at 26 Hz.

Piezoelectric materials are a convenient way to extract energy from vibrating structures. Because these materials exhibit electromechanical coupling, they can convert strain energy to electrical energy and vice versa. Piezoelectric materials have found wide application as low power generators. In the majority of these applications, the energy harvester is attached to a structure, and it extracts energy from ambient vibrations by operating as a base-excited oscillator. Several analytical models have been proposed to quantify the electrical energy that can be generated. Sodano et al. [8] developed an model for a piezoelectric bimorph energy harvesting device, using Hamilton's principle. Umeda et al. [9] investigated the electrical energy generated by a metal ball falling on a plate with a bonded piezoelectric sheet, and proposed an electrical equivalent circuit that described the conversion of mechanical energy into electrical energy in the piezoelectric material. Roundy et al. [10] discussed the operation and analytical modeling of a base-excited energy harvester consisting of a piezoelectric bimorph with a lumped mass attached to its tip. A relationship for power output as a function of input vibration amplitude and frequency was developed. Ottman et al. [11] designed optimal power conditioning electronics for a piezoelectric generator driven by ambient vibrations. Ajitsaria et al. [12] developed mathematical models for the voltage generated by a bimorph piezoelectric cantilever beam, using three different approaches. All the above studies targeted piezoelectric energy harvesters based on ambient structural vibrations. As a result, these devices are inherently limited to relatively low power outputs. Some piezoelectric energy harvesting devices have been developed to harness energy from structural vibrations induced by wind. For example, the energy harvester developed by Tan and Panda [13] is based vibrations excited in a piezoelectric bimorph when exposed to incident wind.

A potential application of energy harvesting from a galloping structure is to power wireless sensors that are commonly used for health monitoring of large civil structures. The availability of low-power micro-sensors, actuators, and radios is enabling the application of distributed wireless sensing to a wide range of applications such as smart buildings, medical applications, and precision agriculture [13,14, 15]. Wang et al. [16] described a prototype wireless sensing system specially designed for structural monitoring of a bridge, which uses batteries as a power source. Mainwaring et al. [17] studied the application of wireless sensor networks to real-world habitat and environmental monitoring such as monitoring seabird nesting environment in an ecological

Contributed by the Technical Committee on Vibration and Sound of ASME for publication in the JOURNAL OF VIBRATION AND ACOUSTICS. Manuscript received October 4, 2010; final manuscript received May 9, 2011; published online December 28, 2011. Assoc. Editor: Wei-Hsin Liao.

 Copyright © 2012 by ASME

Downloaded 28 Dec 2011 to 128.83.63.20. Redistribution subject to ASME license or copyright; see http://www.asme.org/terms/Terms_Use.cfm

reserve. They described the energy requirement for each node to be 6.9 mAh per day. All these applications demonstrate the wide use of wireless sensor network systems that are typically powered by batteries. Replacement of depleted batteries for large network systems is expensive, impractical and environmentally unfriendly. Hence, the use of energy harvesting methods to power the sensors on-site can be beneficial. Because these wireless sensors are all located outdoors, powering them by means of wind energy is a practical alternative to battery power sources.

A piezoelectric energy harvesting device based on a galloping cantilever beam is described in the present work. Such a device has the primary advantages of simplicity and robustness, and could be collocated with the wireless sensors to provide a source of renewable wind energy.

2 Physical Mechanism of Galloping

Consider a prismatic structure with a D-shaped cross-section mounted on a flexible support, exposed to incident wind with a velocity V_∞ along the x-direction as shown in Fig. 1. Initial perturbations generated by the vortices shed from the D-section result in small, periodic oscillations normal to the direction of incident wind, at a frequency that is a function of the Reynolds number. Let the section be moving downward with a velocity y (defined as positive in the positive y-direction). The instantaneous angle of attack α is given by:

$$\alpha = \tan^{-1}\frac{V_a}{V_\infty} = -\tan^{-1}\frac{\dot{y}}{V_\infty} \tag{1}$$

where V_a is the apparent velocity of the incident wind, equal in magnitude and opposite in direction to$\dot{y}$. It is seen that α depends upon the velocity y of the galloping body as well as on the incident velocity. The quasi-steady lift force L and drag force D (per unit length) on the section are given by:

$$L = \frac{1}{2}\rho V_\infty^2 .b.C_l(\alpha) \tag{2}$$

$$D = \frac{1}{2}\rho V_\infty^2 .b.C_d(\alpha) \tag{3}$$

where b is the characteristic length normal to incident flow (chord of the D-section), ρ is the air density, and C_l, C_d are the sectional lift and drag coefficients respectively. Previous research has shown that it is sufficient to include only quasi-steady aerodynamic forces in the analysis, because the characteristic time scale of the system (b/V_∞) is much smaller than the galloping time period [5].

The components of the lift and drag along the y-direction give the instantaneous excitation force per unit length F_y as:

$$F_y = D\sin\alpha + L\cos\alpha \tag{4}$$

Typical 2D (two-dimensional) sectional lift and drag coefficients for a D-section were measured by Ratkowski [18], and are shown in Fig. 2. Note that the angle of attack (plotted along the x-axis) is defined as the angle between the incident wind and the flat face of the D-section. For a D-section oriented as shown in Fig. 1, the angle of attack is close to 90°. In this region, it is seen that the lift coefficient C_l is approximately linear and has a negative slope. The drag coefficient C_d is approximately constant.

The equation of motion of the D-section mounted on a flexible support, having effective mass per unit length of m, a structural damping coefficient ξ and stiffness $m\omega_n$ [2] is basically that of a linear spring mass damper oscillator with the forcing term F_y:

$$m[\ddot{y} + 2\xi_n\dot{y} + \omega_n^2 y] = F_y(\alpha) \tag{5}$$

For small displacements from an equilibrium position,

$$F_y = \frac{\partial F_y}{\partial\alpha}\alpha = \frac{1}{2}\rho V_\infty^2 .b.\left(\frac{dC_l}{dC_d} + C_d\right)\alpha \tag{6}$$

Hence, for small α, Eq. (5) can be written as:

$$m[\ddot{y} + 2\xi_n\dot{y} + \omega_n^2 y] = \frac{1}{2}\rho V_\infty^2 .b.\left(\frac{dC_l}{dC_d} + C_d\right)\frac{\dot{y}}{V_\infty} \tag{7}$$

Equation (7) represents the general equation of motion governing galloping of the structure. It is seen that the forcing term acts as an additional damping due to its dependence on$\dot{y}$. Unstable oscillations, i.e., galloping, occur when the effective damping of the system becomes negative. For low values of structural damping ξ, the condition for galloping to occur can be written as:

$$\left(\frac{dC_l}{dC_d} + C_d\right) < 0 \tag{8}$$

Equation (8) is known as the Den Hartog criterion [1] and can be used to estimate when galloping will occur on any given structure. This criterion depends only on the sectional aerodynamic coefficients; specifically, galloping occurs when

$$\left(\frac{dC_l}{dC_d} < -C_d\right) \tag{9}$$

From Fig. 2, it is seen that this condition is satisfied for the D-section when the incident wind is perpendicular to the flat face. The negative damping coefficient during galloping condition indicates that energy is extracted by the structure from the air stream. This energy can be harvested and used as a power source.

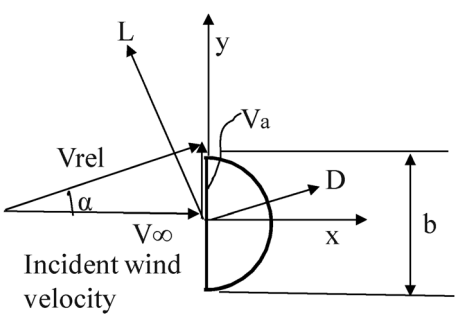

Fig. 1 Forces on a D-section in an incident wind

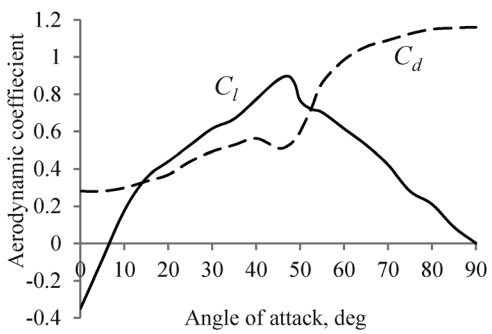

Fig. 2 C_l and C_d plots for a D-section, from Ratkowski [18]. The angle of attack is defined with respect to the flat face.

Downloaded 28 Dec 2011 to 128.83.63.20. Redistribution subject to ASME license or copyright; see http://www.asme.org/terms/Terms_Use.cfm

3 Operating Principle of the Galloping Device

The galloping device developed in this study consists of an aluminum cantilever beam with a tip body consisting of a rigid prismatic bar having a D-shaped cross section. A schematic of the device is shown in Fig. 3. The beam is initially held at rest. The direction of incident wind is normal to the flat surface of the D-section, which corresponds to an angle of attack of 90° as defined in Fig. 2. For angles of attack in this range, the lift curve slope of the D-section is negative, and the Den Hartog criterion is satisfied. As a result, the D-section is prone to galloping. Initial perturbations are caused by vortex shedding and the D-section begins to gallop in a direction transverse to the plane of the beam. The resulting oscillatory bending displacement of the beam progressively increases in magnitude as energy is transferred from the incident wind to the structure. Piezoelectric sheet elements (PZT) bonded to the top and bottom surface of the aluminum beam generate an alternating voltage in response to the bending induced by the galloping D-section. In a practical wind energy harvester, the generated electrical energy would be stored or used to power other devices; however, in the present study, the voltage is simply discharged across a load resistance.

The load resistance across the piezoelectric sheets dissipates energy in the form of Ohmic heating and hence, acts as an additional positive damping on the system. Therefore the amplitude of oscillation of the beam increases till a steady state is reached, wherein the energy extracted from the incident wind is exactly equal to the energy dissipated across the load resistance. In this steady state, the amplitude of oscillation remains constant. For a given incident wind velocity, the induced angle of attack is a function of the beam tip displacement, oscillation frequency, tip slope and location along the tip body.

4 Analytical Model

A coupled electromechanical model of the galloping energy harvesting device is developed from a mechanics based approach, using the coupled electromechanical energy of the system (see Sodano et al. [8], Lee [19], Nisse [20]) The goal of the model is to predict the voltage generated by the PZT as a function of time, for a given incident wind speed, beam geometry and load resistance. The model consists of two parts: the structural model and the aerodynamic model. Devices with different tip bodies can be modeled using different aerodynamic models in conjunction with the same structural model.

4.1 Structural Model. The constitutive equations of a piezoelectric material, relating the strain ϵ and electric displacement D to the mechanical stress σ, and electric field E are given by [21]:

$$\begin{bmatrix} \in \\ D \end{bmatrix} = \begin{bmatrix} s^E & d \\ d^T & e^\sigma \end{bmatrix} \begin{bmatrix} \sigma \\ E \end{bmatrix} \tag{10}$$

where $s^E$is the compliance matrix, e^σ is the matrix of dielectric constants, and d is the piezoelectric coupling matrix. The superscripts E and σ signify quantities measured at constant electric field and mechanical stress, respectively. The potential energy U of the device consists of terms due to mechanical strain energy as well as electrical energy, and is given by:

$$U = \frac{1}{2}\int_{V_s} \sigma^T \in dV_s + \frac{1}{2}\int_{V_P} \sigma^T \in dV_p + \frac{1}{2}\int_{V_P} E^T D dV_p \tag{11}$$

where the quantity V_p indicates the volume of the piezoelectric element and V_s is the volume of the base structure. In the case of the device in the present study, Eq. (11) can be simplified by substituting one-dimensional quantities for stress, strain, electric field and electric displacement, yielding:

$$U = \frac{1}{2}\int_{V_s} \sigma_{11} \in_{11} dV_s + \frac{1}{2}\int_{V_P} \sigma_{11} \in_{11} dV_p + \frac{1}{2}\int_{V_P} E_3 D_3 dV_p \tag{12}$$

Because the coupled energy (as opposed to enthalpy) of the system is being considered, it must be expressed in terms of the basic quantities D and [epsilon]. Dropping the subscripts and substituting for stress and electric field from the piezoelectric constitutive equations gives

$$U = \frac{1}{2}\int_{V_s} Y_s \in^2 dV_s + \frac{1}{2}\int_{V_P} Y_p^D \in^2 dV_p + \frac{1}{2}\int_{V_P} \frac{D^2}{e^\in} dV_p - \int_{V_P} \frac{k^2}{d(1-k^2)} D \in dV_p \tag{13}$$

Where the superscripts D and ϵ refer to quantities measured at constant electric displacement and constant strain, respectively. The electromechanical coupling coefficient of the piezoelectric, k is given by:

$$k^2 = k_{31}^2 = \frac{d_{31}^2 . Y_p^E}{e^\sigma} \tag{14}$$

Note that

$$Y_p^D = Y_p^E (1-k^2) \tag{15}$$

$$e^\in = e^\sigma (1-k^2) \tag{16}$$

Using the Euler-Bernoulli theory for a beam in bending yields the strain at any height y from the neutral axis as:

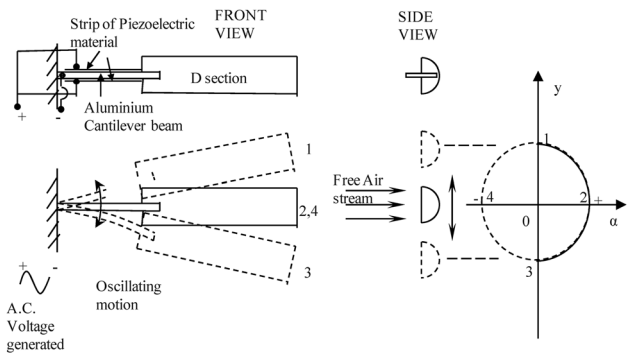

Fig. 3 Schematic of the device showing galloping mechanism and change in instantaneous angle of attack

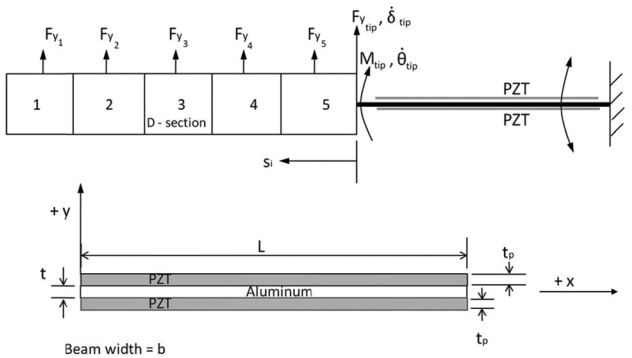

Fig. 4 Schematic of the beam geometry and spatial discretization

Downloaded 28 Dec 2011 to 128.83.63.20. Redistribution subject to ASME license or copyright; see http://www.asme.org/terms/Terms_Use.cfm

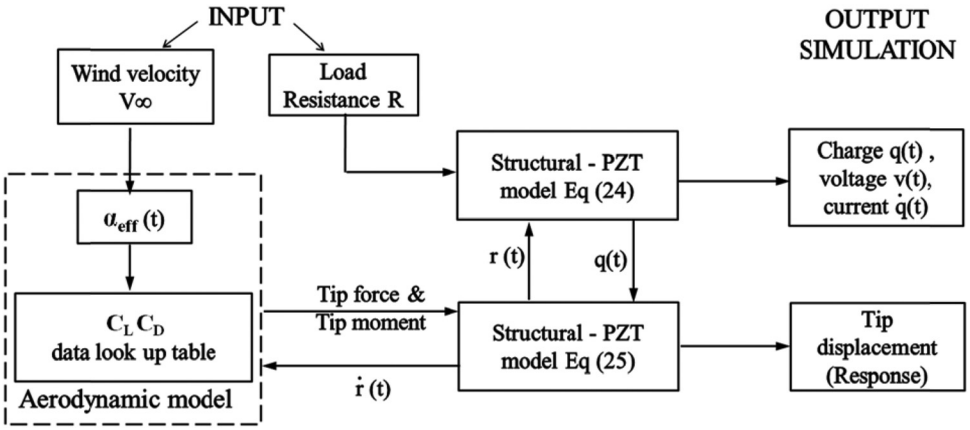

Fig. 5 Block diagram of solution procedure in MATLAB Simulink

$$\in = -v'' y \tag{17}$$

where v'' is the curvature (v is the vertical displacement in the y-direction). The beam displacement v can be assumed as:

$$v(x,t) = \sum_{i=1}^{N} \varphi_i(x) r_i(t) = \varphi r \tag{18}$$

where $\boldsymbol{\varphi}$ is the vector of shape functions set to satisfy boundary conditions, $\boldsymbol{r}$ is the vector of temporal coordinates of displacement and N is the number of modes included in the analysis. The electric displacement is related to the charge generated q and the area of the electrodes A_p by:

$$D = \frac{q}{A_p} \tag{19}$$

Substituting the above expressions into Eq. (13) yields the potential energy of the device as:

$$U = \frac{1}{2}\int_{V_s} Y_S r^T \phi''^T \phi'' r.y^2 dV_s + \frac{1}{2}\int_{V_P} Y_P^D r^T \phi''^T \phi'' r.y^2 dV_p + \int_{V_P} \frac{k^2}{d(1-k^2)A_P} r.y\, dV_p + \frac{1}{2}\int_{V_P} \frac{q^2}{e^{\in} A_P^2} r.y\, dV_p \tag{20}$$

The kinetic energy T is given by:

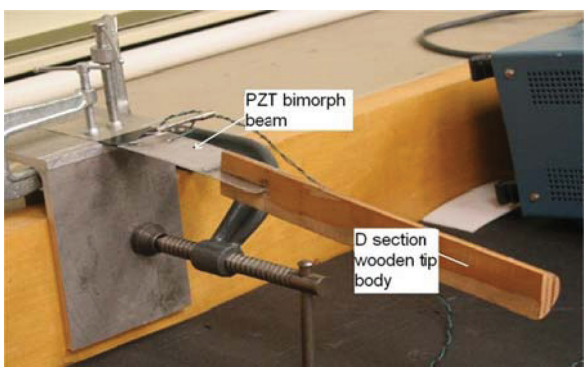

Fig. 6 Experimental setup showing aluminum beam with piezoelectric (PZT) sheets and D-section tip body

$$T = \frac{1}{2}\int_{V_S} \rho_s \dot{v}^2 dV_S + \frac{1}{2}\int_{V_P} \rho_p \dot{v}^2 dV_p + \frac{1}{2} m_{tip} \dot{v}^2(L) + \frac{1}{2} I_{tip} (\dot{v}'(L))^2 \tag{21}$$

The quantities m_{tip} and I_{tip} correspond to the mass and moment of inertia of the tip body, respectively. Substituting for the assumed displacements, we get

$$T = \frac{1}{2}\int_{V_S} \rho_s \dot{r}^T \phi^T \phi \dot{r} dV_S + \frac{1}{2}\int_{V_p} \rho_p \dot{r}^T \phi^T \phi \dot{r} dV_p + \frac{1}{2} m_{\text{tip}} \dot{r}^T \phi(L)^T \phi(L) \dot{r} + \frac{1}{2} I_{\text{tip}} \dot{r}^T \phi'(L)^T \phi'(L) \dot{r} \tag{22}$$

The external virtual work done on the system is given by:

$$\delta W = \delta v(L) F_{\text{tip}} + \delta v(L) M_{\text{tip}} - \delta q.V \tag{23}$$

where F_{tip} and M_{tip} are the external forces and moments acting at the tip of the beam, and V is the voltage across the electrodes on the piezoelectric sheets. The governing equations of the system can be derived from the potential energy, kinetic energy and virtual work either by using Hamilton's principle or by applying Lagrange's equations. The governing equations are:

$$M\ddot{r}(t) + Kr + \Theta^T q = F_{\text{tip}} \phi_{\text{tip}} + M_{\text{tip}} \phi'_{\text{tip}} \tag{24}$$

$$\Theta r + \frac{q}{C_P} = -V \tag{25}$$

In the above equations, the effective mass matrix M is given by:

$$M = \int_{V_S} \rho_s \phi^T \phi dV_S + \int_{V_p} \rho_p \phi^T \phi dV_p + m_{tip} \phi(L)^T \phi(L) + I_{tip} \phi'(L)^T \phi'(L) \tag{26}$$

Table 1 Parameters of experimental setup

Property	Symbol	Value
PZT Strain Coefficient (pC/N)	d_{31}	-320
PZT Young's Modulus (GPa)	Y_p^E	62
PZT Dielectric Constant (nF/m)	e^{σ}	33.645
PZT Density (kg/m^3)	ρ_p	7800
Aluminum Young's Modulus (GPa)	Y_s	70
Aluminum Density (kg/m^3)	ρ_s	2700
Tip Mass (g)	m_{tip}	65

Downloaded 28 Dec 2011 to 128.83.63.20. Redistribution subject to ASME license or copyright; see http://www.asme.org/terms/Terms_Use.cfm

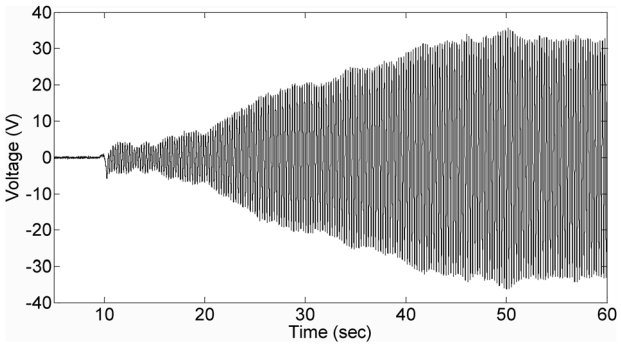

Fig. 7 Measured voltage generated by the piezoelectric sheets, 0.7 MΩ load resistance at wind velocity of 9.5 mph

The effective stiffness matrix K is given by:

$$K = \int_{V_s} Y_S \phi''^T \phi'' y^2 dV_s + \int_{V_P} Y_P^D \phi''^T \phi'' y^2 dV_p \tag{27}$$

A coupling vector Θ can be defined as:

$$\Theta = \int_{V_P} \frac{k^2}{dA_P(1-k^2)} \phi'' y dV_p \tag{28}$$

The capacitance of the piezoelectric sheets, C_p is given by (assuming a uniform cross-section and a piezoelectric sheet of thickness t_p):

$$C_P = \frac{e^{\in} A_P}{t_p} \tag{29}$$

In addition, for the present system, the voltage and charge are coupled together by the load resistance R_L connected across the electrodes of the piezoelectric sheets. This relation can be expressed as:

$$V = iR_L = \dot{q}R_L \tag{30}$$

Equations (24) and (25), in conjunction with the voltage-charge relation given by Eq. (30) represent a coupled electromechanical model of the power harvesting device. To account for structural damping, an additional proportional damping matrix C is incorporated.

$$C = \alpha M + \beta K \tag{31}$$

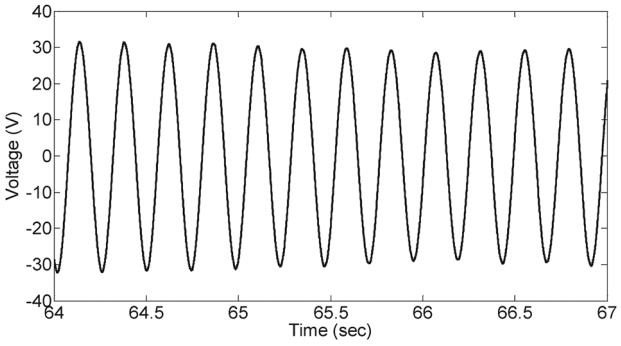

Fig. 8 Measured voltage generated by the piezoelectric sheets at steady state, 0.7 MΩ load resistance at wind velocity of 9.5 mph

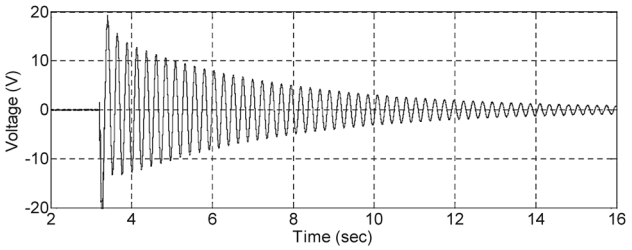

Fig. 9 Measured impulse response of the beam, with electrodes open-circuited

where α and β are determined from:

$$\zeta_i = \frac{\alpha}{2\omega_i} + \frac{\beta\omega_i}{2} \quad \text{i} = 1, 2, ..N \tag{32}$$

In the above equation, ω_i is the natural frequency of the ith mode, ζ_i is the modal damping, and N is the number of modes (equal to the dimension of the mass and stiffness matrices). These quantities are measured experimentally from the impulse response of the beam with an appropriate electrical boundary condition for the piezoelectric sheets.

4.2 Aerodynamic Model. The right hand side of Eq. (24) represents the forcing function. In the case of the present galloping device, the tip of the beam is subjected to aerodynamic force F_{tip} and tip moment M_{tip} that are due to the sectional aerodynamic force F_y integrated over the length L of the tip body. The present analysis only considers quasi-steady aerodynamics and neglects any apparent mass of the air surrounding the structure. The aerodynamic force and moment are given by:

$$F_{tip} = \int_0^L F_y ds = \int_0^L [L\cos(\alpha) + D\sin(\alpha)] ds \tag{33}$$

$$M_{tip} = \int_0^L F_y . s ds \tag{34}$$

where s is the length coordinate along the tip body. Due to the geometry of the device, the sectional angle of attack is a function of rate of change of beam tip displacement, rate of change of beam tip slope and the location of the section along the tip body, and is given as:

$$\alpha(s) = \frac{sy(L) + \dot{y}(L)}{V_\infty} \tag{35}$$

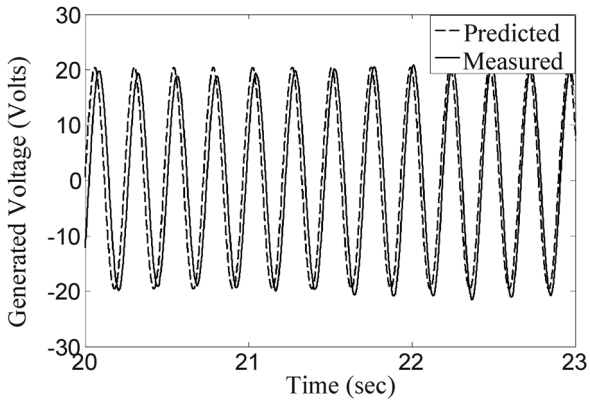

Fig. 10 Comparison of measured and predicted voltage at steady state, 0.7 MΩ load resistance at wind speed of 8 mph

Downloaded 28 Dec 2011 to 128.83.63.20. Redistribution subject to ASME license or copyright; see http://www.asme.org/terms/Terms_Use.cfm

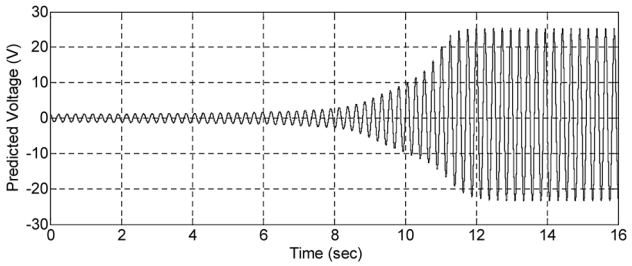

Fig. 11 Transient response of the beam as predicted by analysis, at incident wind speed of 8.6 mph, and 0.7 MΩ load resistance

The sectional lift and drag coefficients were obtained from the data measured by Ratkowski [18] (Fig. 2). Note that the angle of attack α_{eff} required to use this data is related to the angle of attack in Eq. (35) by:

$$\alpha_{\text{eff}}(s) = \frac{\pi}{2} - \alpha(s) \tag{36}$$

4.3 Solution procedure. The constitutive equations of the model [Eqs. (24) and (25)] were solved by time marching using MATLAB Simulink. A single, cubic shape function is assumed to represent the beam deflection as:

$$v(x,t) = \phi(x)r(t) = \left(\frac{x}{L}\right)^3 r \tag{37}$$

where L is the length of the beam. The tip body is discretized into several elements to evaluate the tip force and tip moment as given by Eqs. (33) and (34). The geometry of the beam with piezoelectric sheets and the spatial discretization of the tip body are shown schematically in Fig. 4.

The block diagram shown in Fig. 5 describes the solution procedure. The model predicts beam tip response $v(L,t)$, voltage $v(t)$ generated and current flowing through the load resistance for given values of incident wind velocity, load resistance and device geometry. Tip bodies of any cross-sectional geometry can be evaluated by incorporating the appropriate sectional airfoil characteristics in the form of a table lookup.

5 Experimental Setup

A prototype galloping beam device was constructed and tested to validate the analytical model. The tip body is a rigid wooden bar 235 mm long, with a D-shaped cross section of 30 mm diameter. The bar is attached to the tip of a 90 mm long aluminum cantilever beam, of width 38 mm and thickness 0.635 mm (see Fig. 6). Two piezoelectric sheets (PSI-5H4E from Piezo Systems, Inc. [22]) of length 72.4 mm, width 36.2 mm and thickness 0.267 mm are bonded to the top and bottom surface of the aluminum beam. The piezoelectric sheets are connected in parallel with opposite polarity, because the top layer undergoes tension when the bottom layer is undergoing compression. In this way, the charges developed by the piezoelectric sheets are added together and the effective capacitance is the sum of the capacitances of the individual sheets. The properties of the beam, tip body and piezoelectric sheets are listed in Table 1.

A range of load resistances are connected across the piezoelectric sheets to measure the voltage generated. A NI 9205 data acquisition system in conjunction with Labview was used to acquire the data. A voltage divider circuit was used to scale the generated voltage down to the range of the data acquisition system. The beam was exposed to different wind velocities by placing it in front of a variable speed axial fan. The wind velocity was measured by a digital anemometer. The generated voltage was measured over a range of incident wind velocities for a constant load resistance. The power generated was calculated based on the generated voltage and the load resistance. The generated voltage was measured over a range of load resistances at a constant wind velocity.

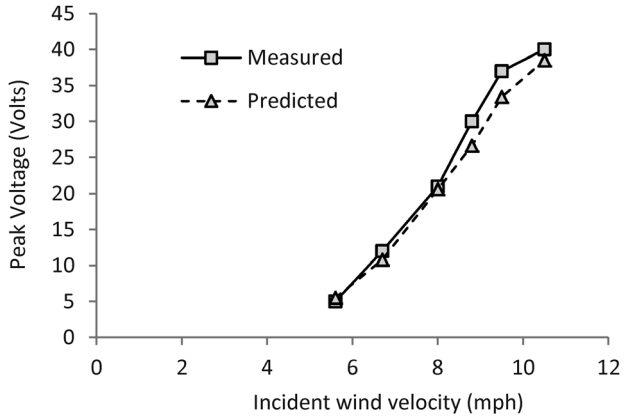

Fig. 13 Comparison of measured and predicted steady state voltage as a function of incident wind velocity, for 0.7 MΩ load resistance

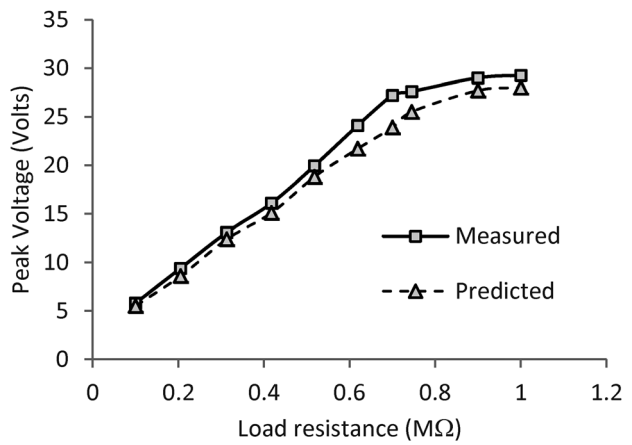

Fig. 12 Comparison of measured and predicted steady state voltage, as a function of load resistance, at wind speed of 8.5 mph

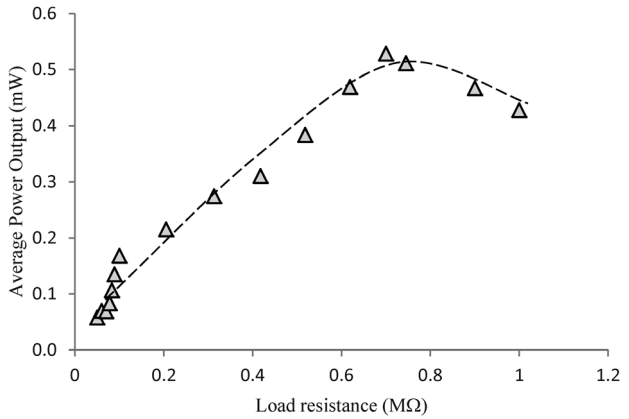

Fig. 14 Measured power as a function of load resistance, at 8.5 mph wind speed

Downloaded 28 Dec 2011 to 128.83.63.20. Redistribution subject to ASME license or copyright; see http://www.asme.org/terms/Terms_Use.cfm

6 Results and Discussion

The focus of the experiments was to measure the bending response of the beam and the voltage generated by the piezoelectric sheets. These data were used to validate the analysis. The influence of various parameters of the system on the power generated was also studied. Figure 7 shows the general trend of measured voltage generated by the piezoelectric sheets starting from rest at a constant incident wind speed. A steady state voltage amplitude of 32 V was measured across a 0.7 MΩ load resistance, at a wind speed of 9.5 mph. This corresponded to a beam tip displacement of approximately 20 mm. Note that although the bending deflection was relatively large, torsional deflections were observed to be minimal. A beam of lower chord may exhibit increased susceptibility to torsion, which may lead to an undesirable change in the angle of attack of the section.

A closer look at the steady state voltage is shown in Fig. 8. It was observed that the response is predominantly a single mode. The frequency of oscillation was found to be constant irrespective of load resistance or wind velocity, and was equal to the natural frequency (4.167 Hz) of the cantilever beam. Note that this result is consistent with the response of a self-excited system, which tends to oscillate at its natural frequency. A major advantage of this kind of response is that the energy harvesting electronics can be optimized to have its peak efficiency at a specific operating frequency.

The mechanical damping ratio ζ of the cantilever beam is calculated from the impulse response of the beam. The voltage generated by the piezoelectric sheets, with open-circuited electrodes, in response to a tip impulse is shown in Fig. 9. From these data, the damping is calculated using the logarithmic decrement.

The measured voltage was compared to that predicted by the analysis for various load resistances and wind velocities. A comparison of the measured and predicted voltages at steady state, for a load resistance of 0.7 MΩ, is shown in Fig. 10. Note that an initial perturbation is introduced in the model to initiate galloping (similar to the effect of the Von Karman vortex street observed in practice) by giving the beam a small tip displacement. A good correlation of both amplitude and frequency is observed. Figure 11 shows the voltage generated by the piezoelectric sheets during the transient response of the beam, as calculated by the analytical model. It is seen that the amplitude of the generated voltage increases with time and then reaches a constant value, qualitatively following the transient response measured experimentally (Fig. 7). It can be concluded that the analytical model can capture both the transient and the steady state behavior of the system. In addition, it can be concluded that quasi-steady aerodynamics are sufficient to describe the forcing on the structure, which was intuitively expected due to the relatively low frequency of oscillation, consistent with previous research [5].

Good correlation is also observed between the measured and predicted steady state voltage amplitudes as a function of load resistance (Fig. 12) and wind speed (Fig. 13). It is seen that the generated voltage increases approximately linearly with the wind velocity for a given load resistance. Note that the voltage generated by the piezoelectric sheets was on the order of 30 V, which implies that small signal electrical characteristics are no longer applicable. This may account for the discrepancies between the predictions and the measured data. Other sources of error could include the effect of the finite thickness bond layer, and discrepancies between the operating conditions (for example, Reynolds number) of the present experimental setup and the experimental setup used for the published aerodynamic coefficients. Although the generated voltage increases with load resistance and wind velocity, the device generates maximum power when the load resistance is optimal. This trend can be seen in Fig. 14. The power plotted is the average power, which is half of the peak power.

The variation of measured power output on wind velocity is shown in Fig. 15, along with analytical predictions. These values correspond to the maximum power output, based on a load resistance of 0.7 MΩ. It is seen that the power output progressively increases with increasing wind velocity. The power output is negligible below a wind velocity of 5.6 mph due to the inherent structural damping in the device. However, annual average wind speed estimates; for example, in region of Texas is around 13 mph [23], which implies that the range of power output shown in Fig. 15 is practically achievable. For the prototype galloping device, a maximum power output of 1.14 mW was achieved at 10.5 mph. Experimental results by Ajitsaria et al. [12] have indicated a maximum power of 250 μW produced by their bimorph PZT bender based on harvesting structural vibrations. It can be concluded that it may be possible to harvest larger amounts of power using galloping devices compared to devices based on structural vibrations.

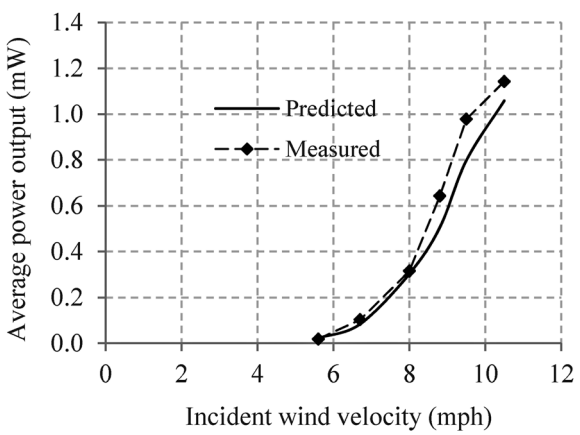

Fig. 15 Measured and predicted output power versus wind velocity, 0.7 MΩ load resistance

7 Summary and Conclusions

A device based on a galloping piezoelectric bimorph cantilever beam was developed to extract power from wind. The beam has a rigid, prismatic tip body of D-shaped cross section that undergoes galloping in an incident wind. Piezoelectric sheets bonded on the beam convert the strain energy into electrical energy.

The electrical power generated by a prototype device 325 mm long was measured over a range of wind speeds, and the feasibility of wind energy harvesting using this device was demonstrated. The power output was observed to increase rapidly with increasing wind speed. Due to the structural damping of the beam, a minimum wind velocity of 5.6 mph was required to generate power from this device. A maximum power output of 1.14 mW was measured at a wind velocity of 10.5 mph.

An analytical model of the device was developed, including quasi-steady aerodynamics for the forcing, aerodynamic properties of the tip body, structural properties of the beam and the electromechanical coupling of the piezoelectric sheets. The analytical model showed good correlation with measured data, and was able to predict both the transient and the steady-state behavior of the device. It was observed that geometry and mass parameters, which determine the natural frequency of the system, play a significant role in the maximum power generated. The good correlation between the analysis and measured data indicates that quasi-steady aerodynamics are sufficient to model the forcing during galloping. Any tip body can be modeled by inputting appropriate sectional aerodynamic data. In this way, a tip body with optimum aerodynamic properties can be designed to maximize the power output of this device. A potential application of power generation using this device is to power wireless sensor devices in large civil structures, exposed to natural wind. It can be concluded that it is possible to harvest significantly more power using this kind of

Downloaded 28 Dec 2011 to 128.83.63.20. Redistribution subject to ASME license or copyright; see http://www.asme.org/terms/Terms_Use.cfm

device compared to a device based on ambient structural vibrations. The device described in this paper forms a baseline for future advancements in development of wind energy based piezoelectric power generators.

Acknowledgment

The authors gratefully acknowledge the Cockrell School of Engineering, University of Texas at Austin, for their start-up grant, and Dr. Ashish Purekar for useful discussions.

References

[1] Hartog, J. P., Mechanical Vibrations (McGraw-Hill, London, 1956), pp. 282–309.
[2] Alonso, G., Meseguera, J., and Pérez-Grandea, I., 2007, "Galloping Stability of Triangular Cross-Sectional Bodies: A Systematic Approach," J. Wind Eng. Ind. Aerodyn., **95**, pp. 928–940.
[3] Kazakevich, M. I., and Vasilenko, A. G., 1996, "Closed Analytical Solution for Galloping Aeroelastic Self-Oscillations," J. Wind Eng. Ind. Aerodyn., **65**, pp. 353–360.
[4] Laneville, A., Gartshore, I. S., and Parkinson, G. V., 1977, "An explanation of Some Effects of Turbulence on Bluff Bodies," *Proceedings of the Fourth International Conference on Wind Effects on Buildings and Structures*, Cambridge University Press, Cambridge, UK, pp. 333–341.
[5] Barrero-Gil, A., Alonso, G., and Sanz-Andres, A., 2010, "Energy Harvesting from Transverse Galloping," J. Sound Vib., **329**(14), pp. 2873–2883.
[6] Robbins, W. P., Morris, D., Marusic, I., and Novak, T. O., 2006, "Wind-Generated Electrical Energy Using Flexible Piezoelectric Materials," *IMECE*2006-14050, ASME Publications-AD, Vol. 71, pp. 581–590.
[7] Wang, D. A., and Ko, H. H., 2010, "Piezoelectric Energy Harvesting from Flow-Induced Vibration," J. Micromechan. Microeng., **20**(2).
[8] Sodano, H. A., Park, G., and Inman, D. J., 2004, "Estimation Of Electric Charge Output For Piezoelectric Energy Harvesting," Strain, **40**(2), pp. 49–58.
[9] Umeda, M., Nakamura, K., and Ueha, S., 1996, "Analysis of The Transformation of Mechanical Impact Energy to Electric Energy Using Piezoelectric Vibrator," Jpn. J. Appl. Phys., **35**, pp. 3267–3273.
[10] Roundy, S., Wright, P. K., and Rabaey, J. M., 2004, *Energy Scavenging for Wireless Sensor Networks with Special Focus on Vibrations*, Kluwer Academic, Norwell, MA, pp. 56, Appendix A.
[11] Ottman, G. K., Hofmann, H. F., and Lesieutre, G. A., 2003, "Optimized Piezoelectric Energy Harvesting Circuit Using Step-Down Converter in Discontinuous Conduction Mode," IEEE Trans. Power Electron., **18**(2), pp. 696–703.
[12] Ajitsaria, J., Choe, S. Y., Shen, D., and Kim, D. J., 2007, "Modeling and Analysis of a Bimorph Piezoelectric Cantilever Beam for Voltage Generation," Smart Mater. Struct., **16**, pp. 447–454.
[13] Tan, Y. K., and Panda, S. K., 2007, "A Novel Piezoelectric Based Wind Energy Harvester for Low-power Autonomous Wind Speed Sensor, Proceedings of the 33th Annual IEEE Conference of Industrial Electronics Society (IECON′07), Taipei, Taiwan.
[14] Estrin, D., Govindan, R., and Heidemann, J., Eds., 2000, "Special Issue on Embedding the Internet," Commun. ACM, **43**(5).
[15] Badrinath, B. R., Srivastava, M., Mills, K., Scholtz, J., and Sollins, K., Eds., 2000, Special Issue on Smart Spaces and Environments, IEEE Personal Communications,
[16] Wang, Y., Kenneth, J. L., Lynch, J. P., Fraser, M., Law, K., and Elgamal, A., 2006, "Vibration Monitoring of the Voigt Bridge using Wired and Wireless Monitoring Systems," The Proceedings of 4th China-Japan-US Symposium on Structural Control and Monitoring, Oct 16–17, Hangzhou, China.
[17] Mainwaring, A., Polastre, J., Szewczyk, R., Culler, D., and Anderson, J., 2000, "Wireless Sensor Networks For Habitat Monitoring," Proceedings of the 1st ACM International Workshop on Wireless Sensor Networks and Applications, Atlanta, Georgia, pp. 88–97.
[18] Ratkowski, J., "Experiments with Galloping Spans," 1961, AIEE Winter General Meeting New York, NY, Paper 62.
[19] Lee, P.C.Y., 1991, "A Variational Principle for the Equations of Piezoelectromagnetism in Elastic Dielectric Crystals," J. Appl. Phys., **69**(11), pp. 7470–7473.
[20] Nisse, E.P.E., 1967, "Variational Method for Electroelastic Vibration Analysis," IEEE Trans. Sonics Ultrason., **SU-14**(4), pp. 153–159.
[21] IEEE Standard on Piezoelectricity, 1987, ANSI/IEEE, Std. 176.
[22] Product Information, 2010, Piezo Systems Inc., 65 Tower Office Park, Woburn, MA 01801,Product Information, 2010, Piezo Systems Inc., 65 Tower Office Park, Woburn, MA 01801, USA, SA, http://www.piezo.com/prodsheet2sq5H.html.
[23] Schwartz, M. N., and Elliot, D. L., "United States Areal Wind Resource Assessment," Report PNL-SA-21606, Presented at the Alternate Fuels and the Environment Symposium, March 28 – April 2, 1993, Denver, CO.

Downloaded 28 Dec 2011 to 128.83.63.20. Redistribution subject to ASME license or copyright; see http://www.asme.org/terms/Terms_Use.cfm